frontiers in Materials

ORIGINAL RESEARCH
published: 25 June 2020
doi: 10.3389/fmats.2020.00116

Tumor-Stroma Interactions Alter the Sensitivity of Drug in Breast Cancer

Virginia Brancato[1,2]*, *Banani Kundu*[1,2], *Joaquim Miguel Oliveira*[1,2,3], *Vitor Manuel Correlo*[1,2,3], *Rui Luis Reis*[1,2,3] *and Subhas C. Kundu*[1,2]*

[1] 3B's Research Group, I3Bs—Research Institute on Biomaterials, Biodegradables and Biomimetics, Headquarters of the European Institute of Excellence on Tissue Engineering and Regenerative Medicine, University of Minho, Guimarães, Portugal, [2] ICVS/3B's–PT Government Associate Laboratory, Guimarães, Portugal, [3] The Discoveries Centre for Regenerative and Precision Medicine, Headquarters at University of Minho, Guimarães, Portugal

Flat cell cultures or xenografts are inadequate tools to unravel cancer complex biology. 3D *in vitro* tumor models garnered interest since they recapitulate better dynamic mechanisms of cancer, but a gold standard model that faithfully mimics solid cancer is not available yet. 3D breast cancer model is fabricated using freeze-dried silk fibroin scaffolds. Breast cancer cell lines (MCF-7 and MDA-MB231) are seeded with normal mammary fibroblasts onto silk fibroin scaffold (1 and 2 mm thick). Cells proliferation is monitored by means of Alamar blue assay. 3D breast cancer models morphology is observed by confocal microscopy. Gene expression modulation concerning extracellular matrix markers is evaluated. Further, 3D bioengineered breast cancer models are treated with doxorubicin. Silk fibroin scaffolds allow the proliferation of cancer cells and fibroblasts. Cells growth is enhanced when cancer cells and fibroblasts are seeded together. Histological staining shows 3D cell organization. MMP-1, MMP-2, MMP-3, Col-1, and Fibronectin expression is upregulated in co-culture. After doxorubicin treatment, stronger reduction in cell activity is observed in 2 mm SF scaffold in comparison to 1 mm. The 3D *in vitro* breast cancer model obtained can easily be scaled-up and translated to the preclinical testing of novel chemotherapeutics.

Keywords: tumor stroma, silk fibroin, 3D cancer models, drug testing, tumor microenvironment

OPEN ACCESS

Edited by:
Antonella Motta,
University of Trento, Italy

Reviewed by:
Yong Yang,
University of North Texas, United States
Lia Rimondini,
University of Eastern Piedmont, Italy

***Correspondence:**
Virginia Brancato
virginia.brancato@i3bs.uminho.pt
Subhas C. Kundu
kundu@i3bs.uminho.pt

Specialty section:
This article was submitted to Biomaterials, a section of the journal Frontiers in Materials

Received: *22 October 2019*
Accepted: *15 April 2020*
Published: *25 June 2020*

Citation:
Brancato V, Kundu B, Oliveira JM, Correlo VM, Reis RL and Kundu SC (2020) Tumor-Stroma Interactions Alter the Sensitivity of Drug in Breast Cancer. Front. Mater. 7:116. doi: 10.3389/fmats.2020.00116

INTRODUCTION

Breast cancer is still a leading cause of death for the European women, especially in Eastern Europe countries. European Commission report states that the death rate for breast cancer was 32.6 per 100000 inhabitants for women in 2014 (European Commission, 2016). Recent studies predict that the number of breast cancer new cases will reach about 3.2 million per year by 2050 (Tao et al., 2015). A massive campaign has promoted prevention and awareness toward this disease in the high-income country. Improved chemotherapeutic treatments are helping to decrease the mortality rate for breast cancer (European Commission, 2016). However, the incidence is increasing throughout Europe due to the spread of some risk factors as sedentary lifestyle, obesity, increased average age of women having their first child and the reduced number of child for each woman. Despite the progress in the chemotherapeutic treatment, breast cancer remains the main cause of cancer-related deaths in Europe (Senkus et al., 2015).

The challenge to defeat breast cancer is also related to the understanding the complexity of the tumor microenvironment (Soysal et al., 2015). Tumor "stroma" is an umbrella term that takes into account the non-tumor cells and extracellular matrix (ECM), while excluding probably the immune cells (Spill et al., 2016). The interplay among different cell types imparts the complexity to the disease (Stadler et al., 2015). Besides cancer cells, the activated fibroblasts (well-known as myofibroblasts or cancer activated fibroblasts, CAFs) are the key cellular component of breast cancer stroma (Miles and Sikes, 2014). The CAFs over-express several ECM proteins including collagens, fibronectin and tenascin C that leads to the ECM stiffening (Madar et al., 2013). The stiffer matrix prompts the invasion of cancer cells into the surrounding tissues (Conklin and Keely, 2012; Klein-Goldberg et al., 2014). Hence, the reactive stroma is actively involved in cancer progression. It is also considered a key regulator of drug sensitivity of cancer cells as reported by recent publications (Östman, 2012; Yuan et al., 2016; Fiori et al., 2019; Qu et al., 2019). Though the research focus in past decade involves the development of therapeutics targeting tumor microenvironment, there is still a lack of understanding how the tumor stromal architecture affect the response of chemotherapeutics. Very limited is known about the relation between cancer stromal architecture and response of anticancer therapeutics, in space and time (Altrock et al., 2018). Hence, in the present work we have employed scaffolds of various thickness to engineer a 3D *in vitro* breast cancer model to investigate the direct effect of scaffold thickness on tumorigenicity and drug response. Silk protein fibroin scaffolds are already used to develop tumor models of breast and hepatocarcinoma, which serve as preclinical *in vitro* platform for drug testing (Talukdar and Kundu, 2012; Kundu et al., 2013a). However, these models do not include the contribution of stromal cells such as fibroblasts or the physical parameters like variable ECM thickness. It is already mentioned that CAFs are of utmost importance for the tumoral progression. An attempt is made to include fibroblasts in 3D *in vitro* tumor model (Dondajewska et al., 2018). This model is used as screening platform for chemotherapeutics. The breast cancer model reported in the work is composed of murine cell lines. It is known that mouse-derived cells cannot be considered as relevant to human cells for the screening of chemotherapeutics for human treatment. A heterotypic breast cancer model based on silk fibroin scaffold is developed by incorporating epithelial and fibroblast cells (Wang and Kaplan, 2012). The same group also investigates the interaction among the breast cancer cells, fibroblasts and adipose cells (Wang et al., 2010). Silk fibroin is also used in combination with other biomaterials (Li et al., 2018). Those breast cancer *in vitro* models can recapitulate the complexity of the tumor microenvironment and the crosstalk among the cells. In this work, we propose a heterotypic breast cancer tumor model, which is obtained by seeding human mammary fibroblasts and two different breast cancer cells lines (MCF-7 and MDA-MB-231) on silk fibroin freeze-dried scaffolds of two different thickness. The morphology and distribution of the cells throughout the silk fibroin scaffolds are detected by mean of scansion electron microscopy, hematoxylin and eosin staining and confocal microscopy. The tumorigenicity of these models are further compared by gene analysis. The engineered 3D *in vitro* breast cancer model is then used as testing platform using cancer drug doxorubicin. The results obtained with homotypic and heterotypic cultures are then compared.

Abbreviations: CAF, Cancer associated fibroblasts; ECM, Extracellular matrix; TGF-β, Tumor growth factor-β; TNF-α Tumor necrosis factor-α; 2D, two-dimensional; 3D, three-dimensional; HMF, Human mammary fibroblasts; 3D-BCM, Three-dimensional breast cancer model; SF, silk fibroin; MMPs, metalloproteinases.

MATERIALS AND METHODS

Materials

Fresh mulberry silkworm (*Bombyx mori*) cocoons were obtained from Portuguese Association of Parents and Friends of Mentally Disabled Citizens (APPACDM, CasteloBranco, Portugal). All other products are purchased from Sigma-Aldrich Company (St. Lewis, USA), if not stated specifically.

Silk Fibroin Scaffold Preparation

Silk protein fibroin was extracted from the silk cocoons. The cocoons after removing the pupae, were cut into pieces before the degumming procedure. To remove glue protein sericin from the silk fibers, the cocoon cut pieces were boiled in a solution of 0.02 M sodium carbonate for an hour. The silk fibers were then washed three times with distilled water to remove sericin residues (Talukdar and Kundu, 2012; Kundu et al., 2013a). Silk fibers were dissolved in a solution of 9.3 M lithium bromide for 1 h at 70°C in an oven. The obtained silk fibroin (SF) solution was dialyzed against distilled water for 48 h using benzoylated dialysis tubing (MWCO: 2 kDa). The final concentration was obtained by measuring the dry weight of SF solution after drying at 70°C in an oven for 24 h. 2 wt % (w/v) SF solution was poured into each well of 96-well plate, which was serving as mold and frozen at −20°C for 48 h. Two different scaffold thicknesses (6 mm in diameter and 1 or 2 mm thickness) were fabricated by pouring 50 or 100 μL of 2 wt% SF solution in each well, respectively. SF scaffolds were obtained after freeze-drying (LyoAlfa 10/15, Telstar, Spain).

Morphological Characterization

Micro-Architectures of 3D Scaffold

The non-porous "skin/ layer" formed at the top surface of each scaffold was removed by simply peeling the skin away immediately post-freeze-drying by using fine-forceps prior to scanning electron microscopy analysis (Rnjak-Kovacina et al., 2015). The morphology of the fabricated scaffold was analyzed by mean of scanning electron microscopy (SEM) (JEOL JSM-6010PLUS/LV). Before the observation, all the samples were sputter-coated with a 3 nm layer of platinum (Sputter Coater SC502, Cressington) and the micrographs were taken at an accelerating voltage of 10 kV at different magnifications. To confirm the interconnectivity of the scaffolds, X-ray microtomography was performed (μCT1272, SkyScan 1272, Belgium). The samples were scanned dry in air with a nominal resolution of ∼2 μm at an intensity of 200 μA, energy of

50 kV and integration time of 1 s. NRecon programme was used to reconstruct the 3D structure, which further investigated morphometrically (CT Analyzer v1.17.0.0, SkyScan, Belgium) for distribution of pores, porosity and pore wall thickness ($n = 3$) (Arya et al., 2012).

Qualitative (Morphological) and Quantitative Characterization: Diffusion

To illustrate the transport of biomolecules or therapeutics within porous SF scaffolds, doxorubicin HCl (DOX, Carbosynth, UK) was prepared in phosphate-buffered saline (PBS) at a concentration of 1 mg/mL and the porous sponges were then placed into the suspension. The diffusion phenomenon was imaged immediately after soaking using an inverted confocal microscope TCS SP8 (Leica Microsystems, Germany). The images are represented as *Z*-stack maximum projection with 50 μm of *Z*-size. To compare the loading and release ability of scaffolds, they were immersed in doxorubicin HCl (500 μg/mL in PBS) and incubated overnight under continuous stirring at 37°C (Cacicedo et al., 2016). The scaffolds were then taken out and the concentration of DOX in supernatant was assayed spectro-fluorometrically. The loading efficiency was evaluated as follows:

$$DOX\ loading\ (\%) = (DOXo - DOXs|DOXo) \times 100$$

Where, $DOXo$ = concentration of DOX at time zero, $DOXs$ = concentration of DOX in supernatant after incubation.

The release of DOX from silk fibroin scaffolds was monitored as a function of time for 7 days in PBS at 37°C. Cumulative drug release was investigated by measuring doxorubicin-associated fluorescence (excitation wavelength 485 nm, emission wavelength 590 nm; Seib et al., 2013).

In vitro Cell Culture

Cells Types

Primary human mammary fibroblasts (HMF) were purchased at Innoprot (Bizkaia, Spain) and grown in fibroblast culture medium supplemented with 1% fibroblast growth factor, 1% antibiotic/antimicotic and 2% FBS (Innoprot). MCF-7 and MDA-MB-231 were purchased from ATCC (Virginia, USA) and cultivated in DMEM high glucose (4.5 g/mL) (Sigma-Aldrich, St. Lewis, USA), 10% (v/v) fetal bovine serum (FBS; Gibco, GB) and 1% (v/v) antibiotic/antimycotic solution (final concentration of penicillin 100 units/mL and streptomycin 100 μg/mL; Gibco, GB). The cells were cultured until 80% confluence at 37°C in 5% CO_2 incubator.

Cell Seeding Onto 3D Silk Fibroin Scaffolds

After the freeze-drying process, the SF scaffolds were soaked in ethanol to induce β-sheet crystallization and insolubility in water (5 min in absolute ethanol). To sterilize the scaffolds, they were soaked in 70% ethanol for 30 min. The scaffolds were washed twice in sterile PBS 1X and sterilized by UV light treatment before the seeding of cells under laminar hood. The day before the seeding, the SF scaffold were transferred in 48 multi-well TCPS plate, soaked in the cell culture medium and left overnight in the CO_2 incubator. Confluent HMF, MCF-7 and MDA-MB231 were detached from the cell culture flasks with TrypLE Express (1X) (Life Technologies, Carlsbad, CA, USA). To carry out monoculture (HMF, MCF-7 and MDA-MB-231), a suspension of 10 μL containing 2×10^5 of each cell type was seeded on the entire top of each scaffold evenly. The seeded scaffolds were allowed to adhere to the scaffold for 3 h at 37°C and 5% CO_2 and then 500 μL of cell culture medium was added in each well. Medium was changed each 3 days and ascorbic acid (50 μg/mL) was added to the HMF culture. The cultures were maintained for 14 days and samples were collected for further analysis at different time point (Day 1, 3, 7, 9, 14). For co-culture models of breast cancer cells and fibroblast, MCF-7 and MDA-MB231 were added at day 7 on the previously HMF seeded scaffold. The density of HMF was 5×10^4 when the co-culture was carried out. To maintain 1:3 ratio between HMF and MCF-7 or MDA-MB-231, the cancer cells were seeded at the density of $1.5x10^5$ cells, at day 7 of the culture. The constructs are referred as 3D-BCM (tridimensional breast cancer model), namely as 3D-HMF, 3D-MCF7, 3D-231, 3D-HMF/MCF7, 3D-HMF/231. Moreover, we classify the 3D-HMF, 3D-MCF7, 3D-231 mono-culture with the term homotypic and the 3D-HMF/MCF7, 3D-HMF/231 co-culture with the term heterotypic.

TABLE 1 | Human primers pairs.

Gene	Primer sequences	Amplicon (bp)	Annealing T (°C)	ID
COL1	Rv–GGCAGTTCTT GGTCTCGTCA	156	59	XM_005257058.4
	Fw–GCCAAGACG AAGACATCCCA			
MMP-1	Rv–TTCAATCCTG TAGGTCAGATGTGTT	248	59	NM_002421.3
	Fw–ACCTGGAAAA ATACTACAA CCTGAA			
MMP-2	Rv – TCAGGTA TTGCACTGCCAACT	169	59	NM_004530.5
	Fw – GCTACGATG GAGGCGTAAT			
MMP-3	Rv–AGTCAGGG GGAGGTCCATAG	81	61	NM_002422.4
	Fw–CACTCACAG ACCTGACTCGG			
Fibronectin	Rv–GCTCATC ATCTGGCCATTTT	230	53	NM_001365524.1
	Fw–ACCAACCTA CGGATGACTCG			
GAPDH	Rv–GTCATGA GTCCTTCCACGA	101	-	NM_001289745.2
	Fw–AGCCTCAA GATCATCAGCAA			
β-actin	Rv—AAGGGACT TCCTGTAACAA	140	-	NM_001101.4
	Fw–CTGGAACG GTGAAGGTGACA			

Cell Viability Assay

The cell viability in the 3D-BCM was assessed by Alamar blue assay (Biorad). 3D-BCM at different time point (Day 1, 3, 7, 9, 14) were incubated with 20% (v/v) Alamar blue solution in DMEM High Glucose without FBS for 4 h at 37°C. The fluorescence was measured using a microplate reader (Synergy HT, BIO-TEK) at an excitation wavelength of 530 nm and an emission wavelength of 590 nm. SF scaffold without cells were used as control.

Cell Morphology in the 3D Silk Fibroin Scaffolds

Confocal Imaging

3D-BCMs were observed by mean of confocal laser microscopy at different time points (1, 7, and 14 days). 3D-BCMs were washed in PBS twice and fixed with 10% (v/v) neutral buffered formalin (Richard-Allan Scientific™, ThermoFisher Scientific, Portugal) for 20 min, permeabilized with 0.2% (v/v) Triton X-100 for 15 min. Actin microfilaments were stained with Phalloidin–Tetramethylrhodamine B isothiocyanate (1:200 in PBS; Sigma-Aldrich, USA) for 45 min and nuclei were counterstained with DAPI (1:1000 in PBS; Sigma-Aldrich, USA) for 10 min. The stained cells were observed by inverted confocal microscope (TSC-SP8, Leica Microsystems, Germany) with diode (405 nm) and HeNe (534 nm) lasers. The samples were observed by using λ_{ex} = 415 nm and λ_{em} = 461 nm to observe cells' nuclei fluorescence, and using λ_{ex} = 560 nm and λ_{em} = 630 nm to observe actin filaments.

Scanning Electron Microscopy

The cell morphology in the 3D-BCM was observed at day 14 by mean of SEM. The constructs were washed in PBS and fixed with a 2.5% (v/v) glutaraldehyde solution overnight at 4°C. Samples were further dehydrated through increasing ethanol concentrations (30, 50, 70, 90, 100% v/v) for 1 h, and left in ethanol absolute overnight. The samples were undergone a cycle of critical point drying (Critical Point Dryer, Autosandri-815, Series A, Tourisms). Before SEM observation, all the samples were sputter coated with gold (Sputter Coater

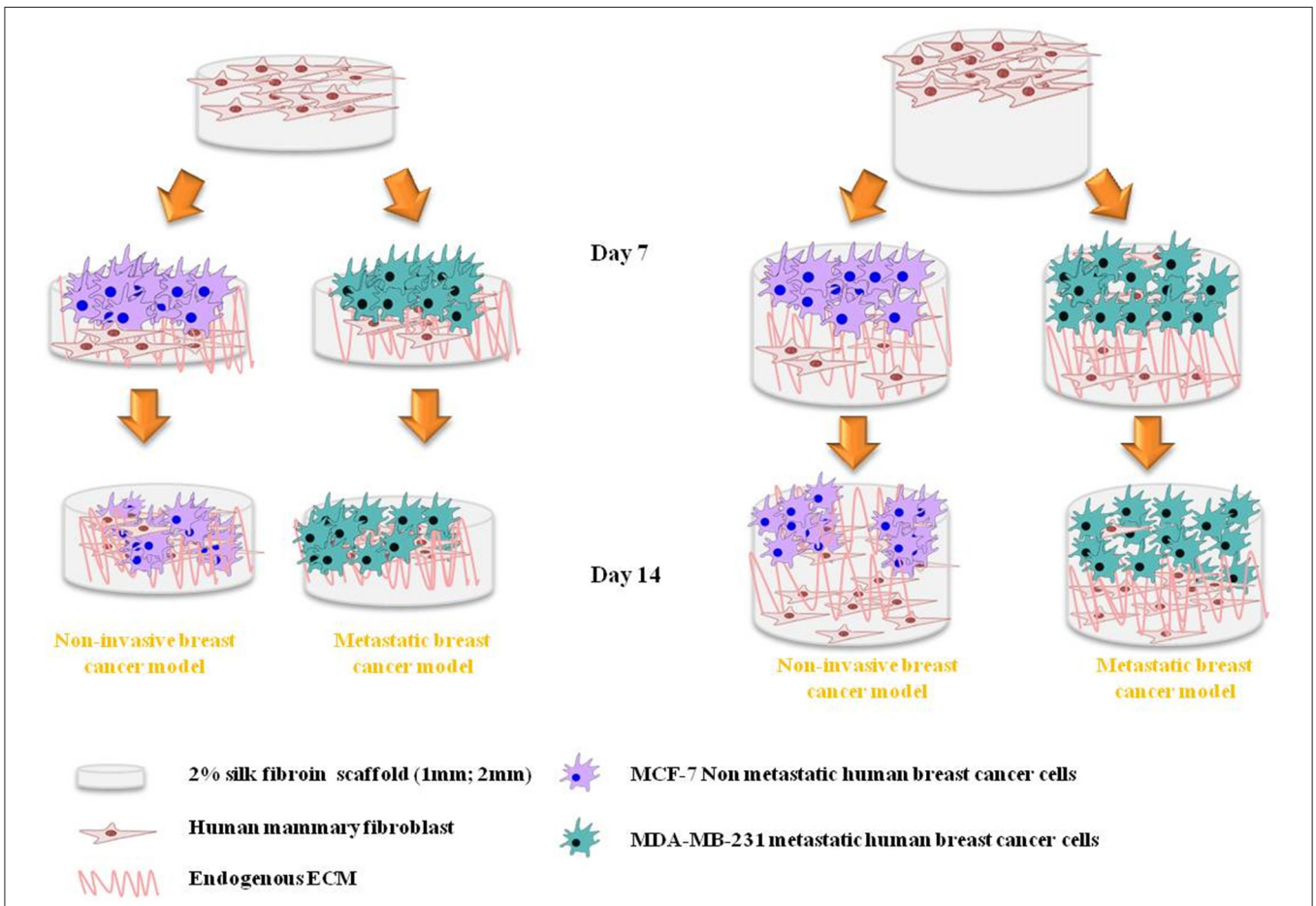

FIGURE 1 | Schematic representation of the *in vitro* cell culture approach using silk protein fibroin (SF) biomaterial to obtain 3D breast cancer model. Silk fibroin scaffolds of two different thicknesses support the growth of breast cancer cells co-cultured with mammary fibroblasts. The cancer cells were seeded 7 days after the fibroblasts seeding. Four different co-cultured conditions were analyzed in this work: 3D-HMF/MCF7 in 1 mm and 2 mm SF scaffold, 3D-HMF/231 in 1 mm and 2 mm SF scaffolds.

SC502, Cressington) and the microphotographs were taken at an accelerating voltage of 10 kV at different magnifications under SEM (JEOL JSM-6010PLUS/LV).

Hematoxylin/Eosin Staining of Silk Fibroin-Cell Scaffold Constructs

To investigate the cell distribution in the 3D-BCM, hematoxylin/eosin staining was carried out. Briefly, the constructs were washed twice in PBS 1X and fixed with 10% (v/v) neutral buffered formalin (Richard Allan Scientific^{TM}, ThermoFisher Scientific, Portugal) for 20 min. The samples were maintained in PBS 1X, dehydrated through increasing ethanol concentrations and embedded in paraffin using an automatized process (EC350-2, Microm, Thermo Scientific, Waltham, MA, USA). Successively, the samples were sectioned at a thickness of 7 μm using a microtome (HM355S, Microm, Thermo scientific, Portugal). Hematoxylin/eosin (Bio-optica, Italy) staining was carried out according to manufacturer's procedure through an automatized process (HMS, Microm, Thermo Scientific, Portugal). The stained structures were mounted with Entellan® (Inopat) and visualized under the microscope with an attached camera (Leica DM750, Germany).

RNA Isolation and Real-Time RT-PCR

SF scaffolds with 1 mm and 2 mm thickness were seeded with $2x10^5$ cells, as described in the section 2.4.2. 3D-BCMs were collected at day 14 to investigate the mRNA expression of the genes of interest. Total mRNA was extracted using TRI Reagent® RNA Isolation Reagent (ThermoFisher Scientific, Portugal), according to the manufacturer's guidelines. RNA concentration and purity were measured by mean of Nanodrop® ND-1000 spectrophotometer (ThermoFisher Scientific, Portugal). The synthesis of cDNA was carried out from 100 ng of mRNA using qScriptTM cDNA Synthesis Kit (Quanta BioSciences, USA). Briefly, a reaction mixture consisting of 4 μL qScript Reaction Mix, 1 μL qScript Reverse Transcriptase (RT), RNA template (100 ng total RNA) and nuclease-free water was prepared in 20 μL of final volume. The single-strand cDNA synthesis occurred by incubating the complete reaction mixture for 5 min at 22°C, followed by 30 min at 42°C and terminated with an incubation of 5 min at 85°C. RT-PCR was performed using PerfeCTA® SYBR Green FastMix (Quanta BioSciences, USA), following manufacturer's instructions, on RT-PCR Mastercycler Realplex machine (Realplex, Eppendorf, Germany). Primer sequences (Eurofins Genomics, UK) were designed using Primer-BLAST tool (**Table 1**). Livak's method ($2^{\Delta\Delta Ct}$) was used to quantify the relative gene expression (Livak and Schmittgen, 2001). The mRNA expression was first normalized to the average expression of multiple internal control genes [glyceraldehyde-3-phosphate dehydrogenase (*GAPDH*) and β-actin (*ACTB*)]. Three samples of each condition were considered and the results are represented as fold change toward the gene expression in the 3D-HMF.

Drug Testing and Cytotoxicity on 3D-BCM

Scaffolds with 1 and 2 mm thickness were seeded with 2×10^5 cells, as described in the section Cell Seeding Onto 3D Silk Fibroin Scaffolds. At day 14, 3D-BCMs (3D-HMF, 3D-MCF7, 3D-231, 3D-HMF/MCF7; 3D-HMF/231) were treated with 15 and 30 μg/mL of DOX (Carbosynth, UK). After the DOX treating for 24, 48, and 72 h at 37°C and 5% CO_2, metabolic activity and cell proliferation were assayed. To evaluate the metabolic activity of the cells in the 3D-BCMs after doxorubicin treatment, Alamar blue assay was performed according to the protocol described in the section Cell Viability Assay. To evaluate cell proliferation in the 3D-BCM after DOX treatment, the amount of DNA of each was quantified by Quant-iT^{TM} PicoGreen® dsDNA assay (Thermofisher scientific, Portugal), according to the manufacturer's guidelines. At each time point, the 3D-BCMs used for the Alamar blue assay were washed twice with PBS, incubated in 1 ml of ultrapure water for 1 h at 37°C and kept at −80°C for further analysis. The constructs were thawed at RT and sonicated 20 min to trigger the membrane lysis. The samples were incubated 10 min in the dark with fluorescent Picogreen® dye. The fluorescence of the supernatant was measured using a microplate reader at 485 and 530 nm excitation and emission wavelength, respectively. SF scaffolds without cells were used as control. To calculate the DNA amount in each sample, the data obtained from the assay were plotted together with the values of DNA concentration and fluorescence of a standard curve ranging between 0 and 2 μg/mL.

Statistical Analysis

To determine statistical significance, the data were analyzed using GraphPad Prism v5.01 software (GraphPad Software, La Jolla, CA). All statistics were reported as mean ± standard deviation. One-way ANOVA test was used to compare the data, followed by Tukey's test. All the experiments were performed in triplicate and statistical significance was considered at $p<0.05$.

RESULTS

The aim of this work is the development of an *in vitro* 3D breast cancer model based on co-cultured primary normal human mammary fibroblasts (HMF) and two different types of breast cancer cells (MCF-7 and MDA-MB231). Two cell types were chosen to mimic different stages of breast cancer like early stage and invasive phenotypes. The chosen scaffold type is 2 wt% silk fibroin (SF) freeze-dried scaffolds of two thickness (1 or 2 mm). The schematic representation (**Figure 1**) shows the approach followed for the development of the 3D-BCM. Briefly, normal mammary fibroblasts were seeded on the SF scaffold. At day 7 of culture, breast cancer cells, MCF-7 and MDA-MB231, respectively, were added into the fibroblast-laden scaffolds and cultured until day 14. Mono-cultures (3D-HMF, 3D-MCF7, 3D-231) were used as control to investigate how the interplay between the cancer cells and fibroblasts could affect the tumor growth or the response to Doxorubicin treatment.

Silk Fibroin Scaffold Preparation and Characterization

Porous SF scaffolds of different thickness were obtained by freeze-drying of different volumes of silk solution (2 wt%) (**Figures 2A,B**). **Figures 2B,C** represent the side and top views, respectively, which reveal highly porous interconnected nature

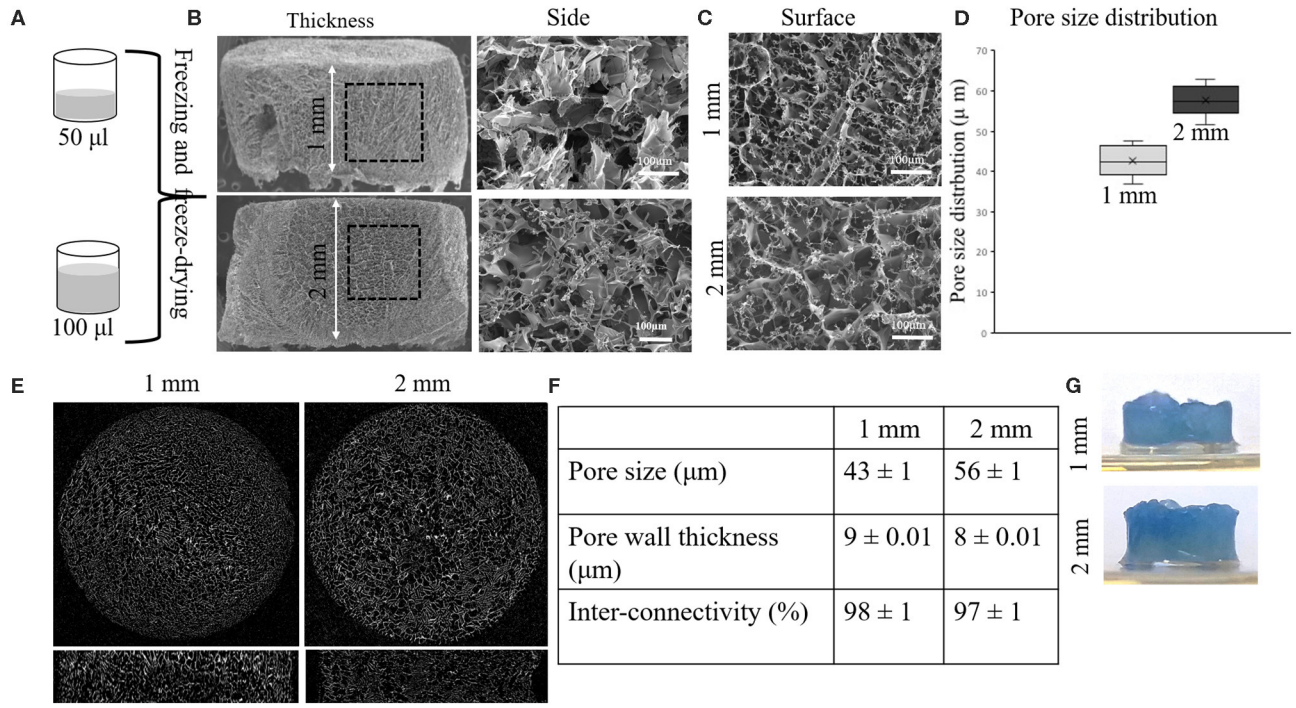

	1 mm	2 mm
Pore size (µm)	43 ± 1	56 ± 1
Pore wall thickness (µm)	9 ± 0.01	8 ± 0.01
Inter-connectivity (%)	98 ± 1	97 ± 1

FIGURE 2 | Silk fibroin (SF) scaffolds' morphological characterization and diffusion. SF scaffolds are obtained pouring 50 µL and 100 µL of silk fibroin solution (2 wt %) in a 96 TCPS well plate **(A)**. Full side **(A,B)** and high view (200× magnification, scale bar 100 µm) of SF 1 and 2 mm scaffolds are shown, respectively. Micrographs **(C)** show the surface profile of the SF scaffolds. The graphs represent the pore size distribution in the two types of SF scaffolds (1 mm and 2 mm). **(D)** The pore size distribution is plotted in the graph. Micrographs **(E)** exhibit the interconnectivity of the porous network in the scaffold with the relative value **(F)** for the pore size, pore wall thickness and inter-connectivity obtained by means of Micro CT analysis ($n = 3$). Alamar blue dye is used to demonstrate liquid diffusion within the scaffolds **(G)**.

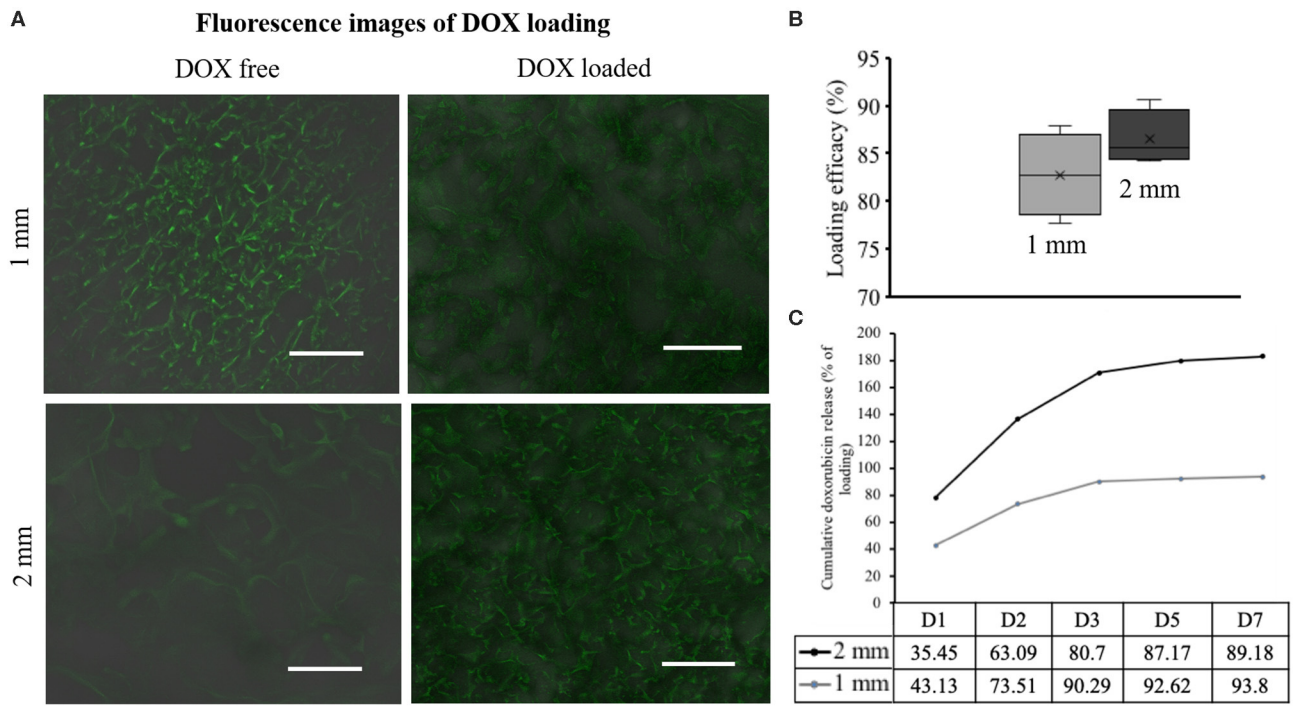

	D1	D2	D3	D5	D7
2 mm	35.45	63.09	80.7	87.17	89.18
1 mm	43.13	73.51	90.29	92.62	93.8

FIGURE 3 | Diffusion profile of doxorubicin (DOX) in the Silk fibroin (SF) scaffolds. DOX is loaded in the SF scaffold and the confocal images are shown together with a DOX free scaffold. It is evident from the SF auto-fluorescence **(A)**. Loading efficiency in both 1 and 2 mm scaffolds is evaluated **(B)**. Cumulative DOX release curve represents the DOX release along 7 days, which is measured by mean of spectrophotometric technique ($n = 3$) **(C)**.

of SF scaffolds. The gradient distribution of pores across the scaffold thickness was due to ice crystal formation and freeze-drying process (Arya et al., 2012). The pore sizes obtained from Micro CT were 43 ± 1 μm and 56 ± 1 μm, respectively (**Figure 2**). The thickness of pore wall was decreased with the increased pore size. Both the scaffolds exhibited well-interconnectivity (> 95%) (**Figure 2F**). To further demonstrate the pore interconnectivity, the SF scaffolds were rehydrated in PBS and placed within a dish containing Alamar blue dye (Rnjak-Kovacina et al., 2015). Instantly upon contact with Alamar blue dye, the scaffolds appeared blue despite being hydrated in PBS (**Figure 2G**). The uptake of dye readily by the scaffolds indicated the interconnectivity within sponges. **Figure 3A** shows the representative confocal microscopy images of porous SF scaffolds with or without doxorubicin (DOX). In order to measure the diffusion properties of scaffolds, the loading of DOX was carried out (for easy visualization due to auto-fluorescence nature of DOX). The diffusion of DOX immediately after immersion was imaged (**Figure 3A**), which indicated the diffused fluorescence signal throughout the porous scaffolds. However, the time-dependent quantitative analysis of DOX diffusion into the porous matrix was not possible to perform due to high loading efficacy. The loading efficacy can be defined as the percentage amount of DOX loaded/entrapped within porous silk fibroin scaffold after initial exposure to free drug and was observed > 80% for both sponges (**Figure 3B**) that corresponding to excessive fluorescence signal (the autofluorescence of silk also provided some background). The release of DOX from scaffolds was defined in relation with their thickness. The release was relatively slow for 2 mm scaffolds, resulting a cumulative release of 89%

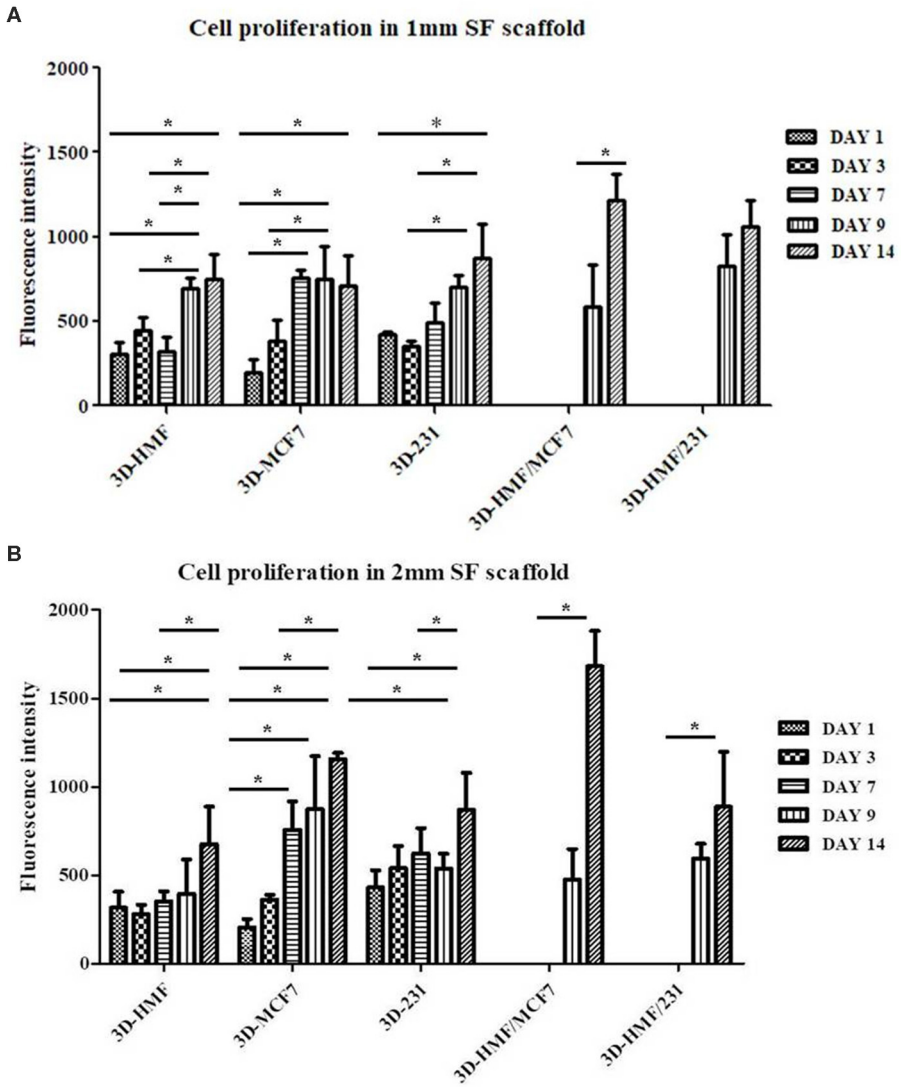

FIGURE 4 | Cell proliferation profile in 1 **(A)** and 2 mm **(B)** Silk fibroin (SF) scaffolds. The cells proliferation is investigated at different time points (Day 1, 3, 7, 9, 14) for both homotypic and heterotypic 3D-BCMs by mean of Alamar blue assay. *$P < 0.05$ is considered as statistically significant ($n = 3$).

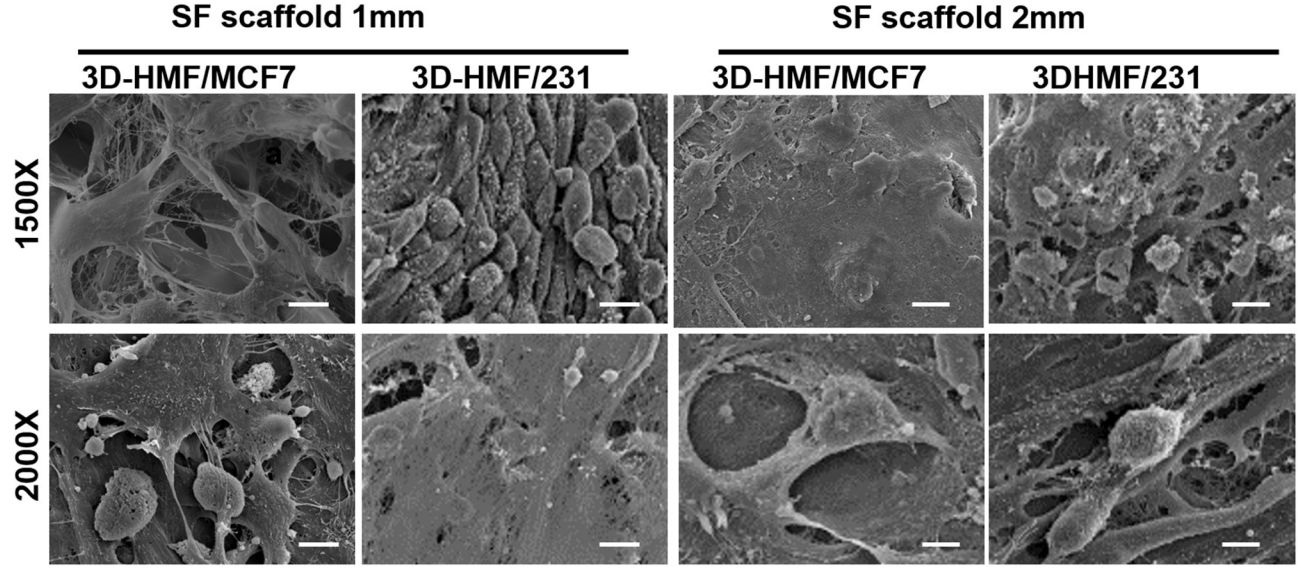

FIGURE 5 | Scanning electron micrographs of the developed 3D tumor models. 3D-HMF/MCF7 and 3D-HMF/231 in 1 mm and 2 mm SF scaffolds are fixed in 2.5% glutaraldehyde at day 14 of co-culture. The scale bar is 10 μm for the 1,500× magnification and 15 μm for the 2,000× magnification micrographs.

after 7 days compared to 1 mm ones, ∼93% (**Figure 3C**). For both types of scaffolds the rapid release of DOX was observed over the first 48 h and this was 73 and 63% of total cumulative release from 1 or 2 mm, respectively. The release was dropped over the remaining period of study.

Cell Viability and Distribution Within Silk Fibroin Scaffolds

Alamar blue assay was carried out to assess the viability and metabolic activity of the cells within the scaffold at different time point (Day 1, 3, 7, 9, 14). The metabolic activity of cells increased along with the time when cells were cultured in both 1 mm and 2 mm silk fibroin scaffolds. In both cases, the heterotypic model showed a higher proliferation rate in comparison to the homotypic one (**Figure 4**), with high growth peak at day 14 for 3D-HMF/MCF7 in 2 mm SF scaffold. We do not observe a significant difference in cell growth when the cells were seeded in 1 or 2 mm thickness scaffolds. The cells showed a rounded shape in the SF scaffold according to the SEM micrographs (**Figure 5**). The cell morphology and distribution were further investigated by mean of Hematoxylin/Eosin staining. Both SEM micrographs and micro-tumor sections revealed a 3D rearrangement of the tumor cells in the scaffolds (**Figure 6A**). The HMF/MCF-7 cells formed compact aggregate in the SF scaffold resembling the 3D architecture of a tumor mass. The HMF/MDAMB231 cells were more spread in the SF scaffolds of both thicknesses (1 mm and 2 mm). Confocal images showed the higher cellular density in the heterotypic 3D-BCM, which also confirmed by the metabolic activities increments. HMF maintained a more spread and elongated shape while the cancer cells (MCF-7 and MDAMB-231) exhibited rounded shape (**Figure 6B**). The Z-scanning of the constructs (i.e. cell laden silk scaffolds of different thickness) indicated the invasion of cells within the interconnective porous scaffolds. Moreover, the cells penetrated both scaffolds irrespective of their thickness. The morphology and dissemination of the cells throughout the scaffolds were also confirmed by micrographs from SEM observation.

Cytotoxicity of DOX in 3D-BCM

At day 15 of culture, the 3D-BCM were challenged with two different concentrations of DOX (15 and 30 μg/mL) as illustrated by the experimental timeline (**Figure 7A**). The DOX cytotoxicity against the 3D-BCM was evaluated at three different time points (24, 48, 72 h). Cell metabolism was evaluated by mean of Alamar Blue assay. In 1 mm SF scaffold, we observed a reduction of the cell metabolism in the 3D-HMF/MCF7 and 3D-HMF/231 co-culture in comparison to the respective 3D-MCF7, 3D-231 monoculture at day 14 (**Figures 7B,C**). Moreover, it is interesting to observe that the 3D-HMF/231 metabolism both in 1 mm and 2 mm SF scaffold was slightly higher than the 3D-HMF/MCF7 one at the three time-points selected for the analysis (**Figures 7B–G**). It is interesting to report that we obtain a time/dose-related response when heterotypic 3D-BCM were treated with DOX at the concentration of 30 μg/mL in the 2 mm SF scaffold (**Figures 7F,E**). In the 2 mm SF scaffolds, the metabolic activity of the 3D-HMF/231 is higher than the 3D-231 monoculture. Double-stranded DNA content was evaluated after DOX treatment in co-cultures (**Figures 7D,E** for 1 mm scaffold and **Figures 7H,I** for 2 mm SF scaffolds) by mean of PicoGreen DNA assay. However, if the percentage of DNA content is calculated, the reduction is not strong when we compared the monocultures and cocultures in 1 mm SF scaffolds (**Figures 7D,E**). The results demonstrated a stronger reduction in DNA content when cells were cultured in 2 mm SF scaffolds in comparison to 1 mm. The results were

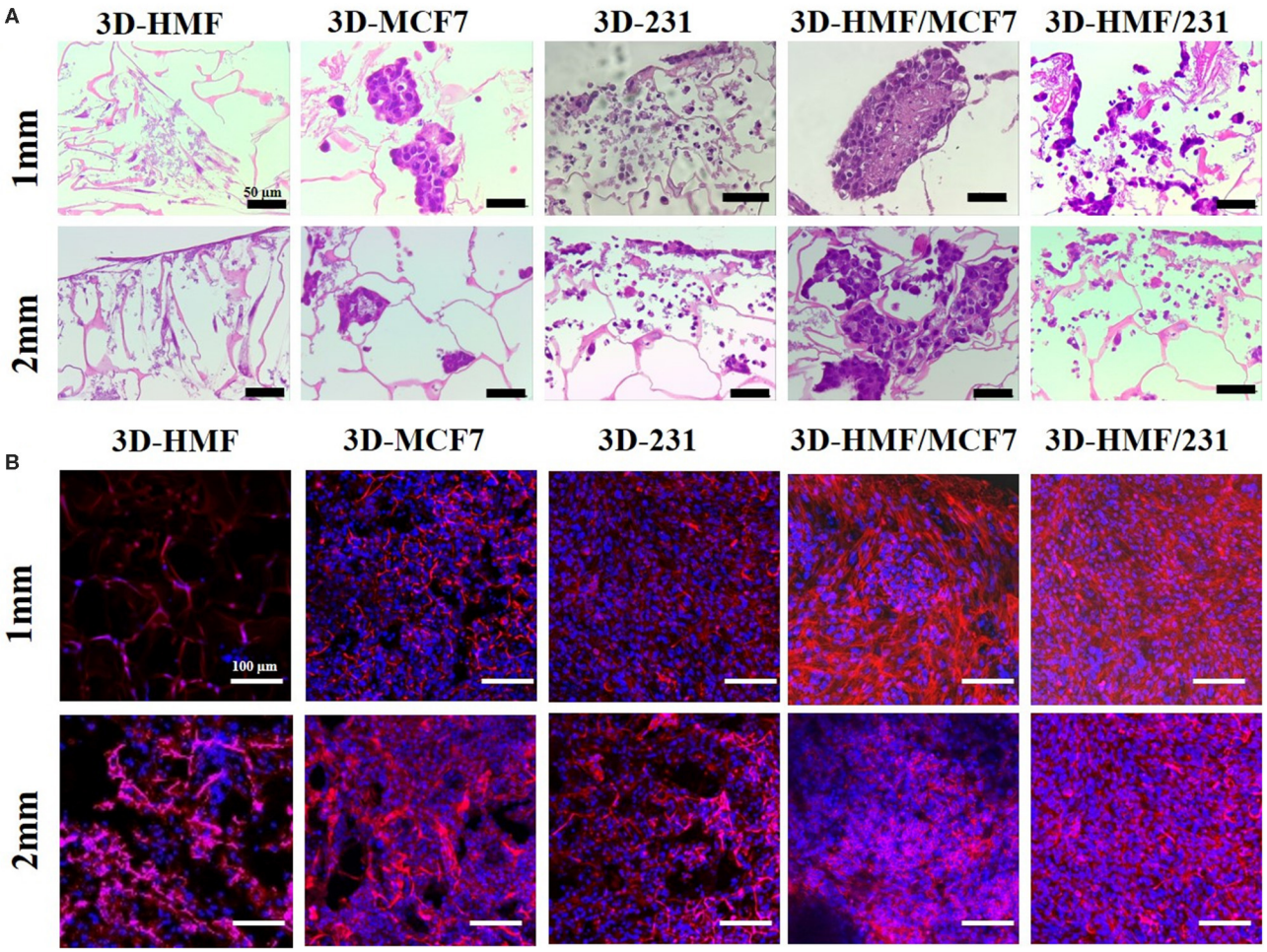

FIGURE 6 | Hematoxylin/eosin staining of developed 3D tumor models constructs at day 14 in both homotypic and heterotypic condition. **(A)** Shows representative images of the 3D-BCM: tumor cells are arranged in spheroid-like architecture (3D-MCF7 and 3D-HMF/MCF7). MDAMB-231 cells spread along the scaffold and do not show an acinar structure (Scale bar 50 µm). **(B)** Representative image of nuclei and cytoskeleton, respectively, stained by DAPI (blue) and Phalloidin (red) (Scale bar 100 µm). The images showed a higher density of cells in heterotypic 3D-HMF/MCF7 and 3D-HMF/231. All the images refer to day 14 of cell culture.

also dose-dependent, showing more decrease in heterotypic cultures in 2 mm SF scaffolds treated with 30 µg/mL of DOX (**Figure 7I**). In 2 mm SF scaffolds, the DNA content is higher in cocultures than in monocultures (**Figures 7H,I**). If only monocultures are considered, both cell metabolism and DNA content decreased in 3D-MCF7, and 3D-231 cultured onto 1 mm SF scaffold. Reduction in DNA content in 2 mm SF scaffolds was higher than in 1 mm SF scaffold (**Figures 7F–I**). The highest decrease in DNA content is reached when 3D-231 in 2 mm SF scaffold is challenged with 30 µg/mL for 72 h (**Figure 7I**).

Gene Expression Profiling in 3D *in vitro* Breast Cancer Model

The expression of genes related to the tumor microenvironment was analyzed. Gene expressions in tumor homotypic and heterotypic cultures were normalized to the homotypic culture of normal mammary fibroblasts (3D-HMF) (**Figure S1**). The up-regulation of Col-I and Fibronectin in the 3D-HMF/MCF-7 and 3D-HMF/231 in comparison to 3D-MCF-7 and 3D-231, both in 1 mm and 2 mm thickness SF scaffolds, is quite relevant. An interesting trend is observed for fibronectin modulation: in 1 mm SF scaffolds, fibronectin level is lower in 3D-HMF/231 when compared to 3D-HMF/MCF-7, while this difference is not statistically significant in 2 mm SF scaffold. MMP-2 is upregulated in both 1 mm and 2 mm SF scaffolds, where 3D-HMF/MCF-7 showed a higher fold change when compared to 3D-HMF/231. In 1 mm SF scaffold, we observed a downregulation of MMP-1 and MMP-3 in co-cultures in comparison to mono-culture, while MMP-2 expression is higher in 3D-HMF/MCF-7 and 3D-HMF/231 in comparison to mono-culture. Regarding the 2 mm SF scaffold, the expression of MMP-1, MMP-2, MMP-3, Col-1 and Fibronectin is slightly higher in co-culture than in mono-culture. If we compare

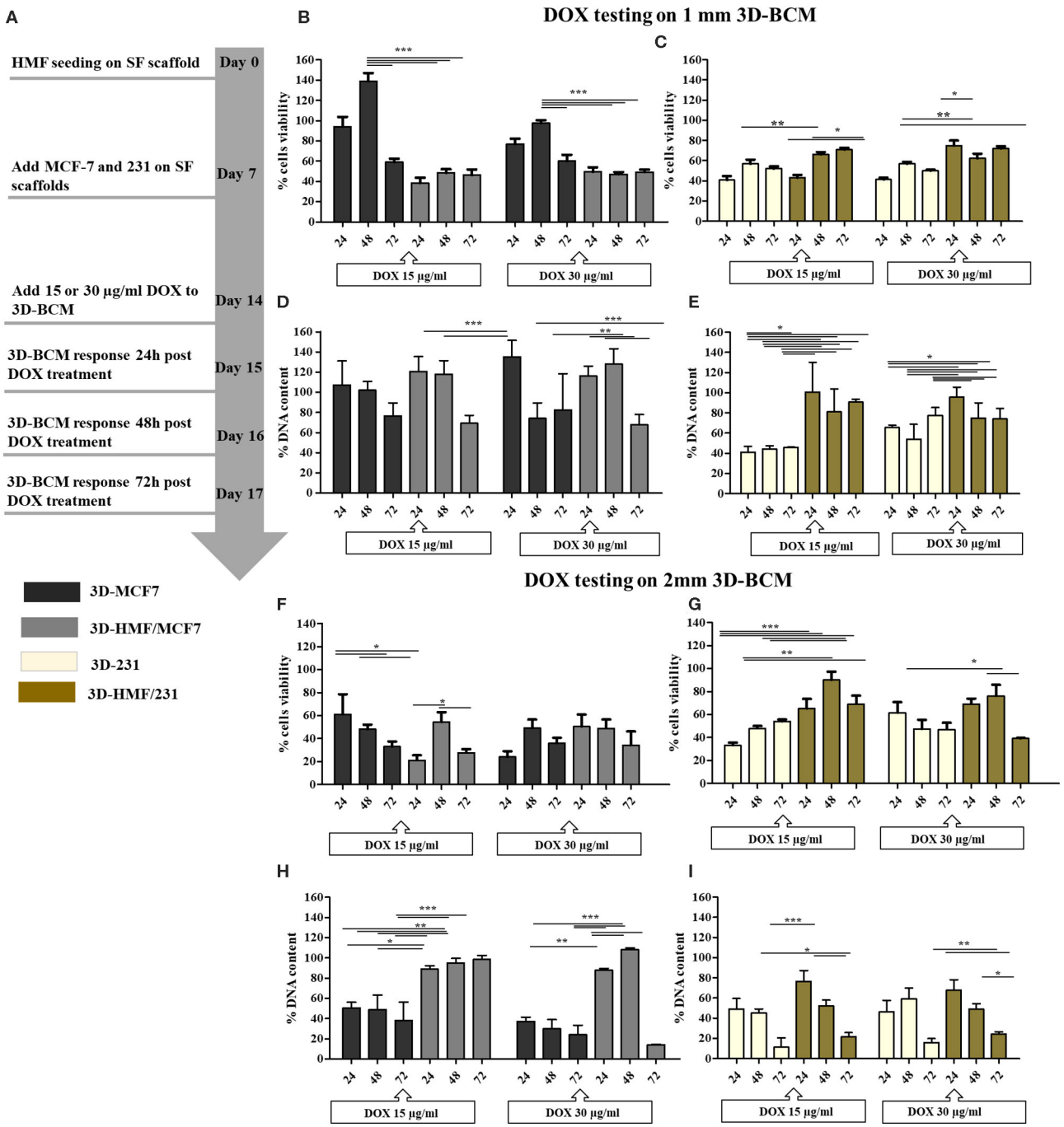

FIGURE 7 | DOX treatment on heterotypic 3D breast cancer model. **(A)** Schematic experimental workflow for the drug testing set-up. The DOX activity is evaluated at 24, 48, and 72 h, starting on day 14 of 3D culture. Anti-proliferative effects of DOX on 3D-MCF7 and 3D-HMF/MCF7 **(B,F)** and 3D-231 and 3D-HMF/231 **(C,G)** was measured by mean of Alamar blue assay in 1 and 2 mm SF scaffolds, respectively. Graphical representation of the amount of double stranded DNA (dsDNA) detected in 3D-MCF7 and 3D-HMF/MCF7 as well as in 3D-231 and 3D-HMF/231 after 24, 48, and 72 h of DOX treatment [**(D,E)** for 1 mm plus **(H,I)** for 2 mm SF scaffolds]. $P < 0.05$ (*) is considered as statistically significant. $^{**}p < 0.01$, $^{***}p < 0.001$ ($n = 3$).

the fold change of the MMP-1 and MMP3 expression in 3D-HMF/MCF-7 and 3D-HMF/231 is higher when the cells were seeded onto 2 mm thickness SF scaffolds in comparison to 1 mm ones.

DISCUSSION

Reliable 3D *in vitro* models can unravel cancer complexity, since they may recapitulate the interactions among the cells of

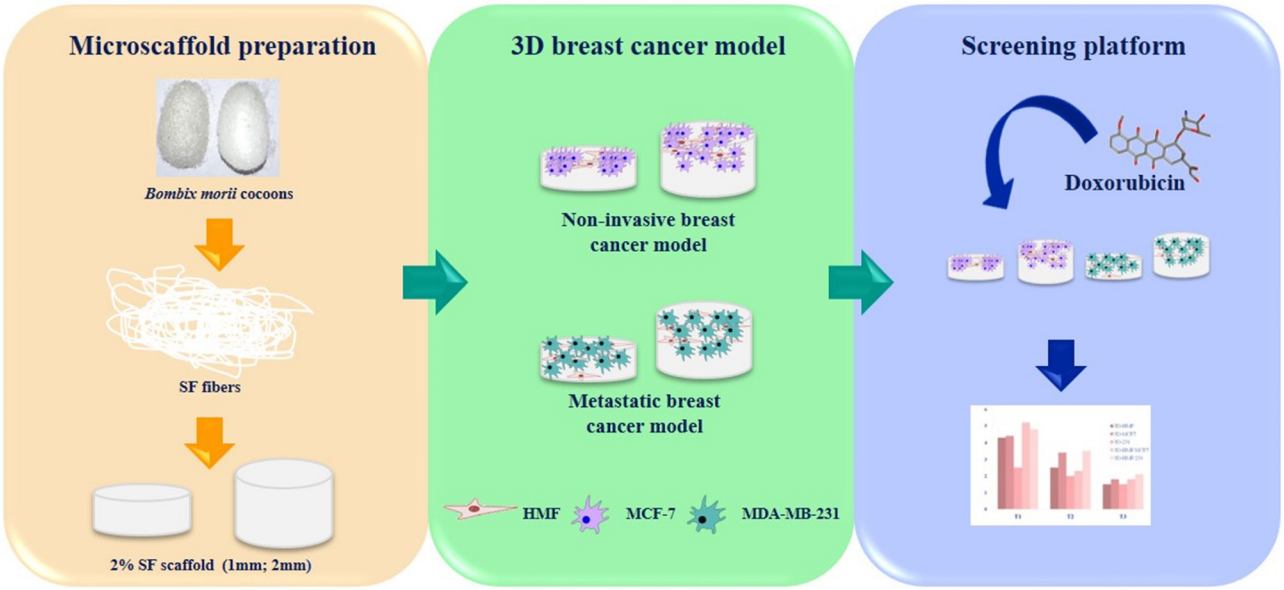

FIGURE 8 | Graphical summary of the experimental setting. Silk fibroin scaffolds are used as matrix to grow different breast cancer cells lines together with mammary fibroblast. The 3D tumor models are challenged with doxorubicin to demonstrate the effect of tumor - stroma cells to the drug response.

the tumor microenvironment (Caballero et al., 2017; Ferreira et al., 2018; Rodrigues et al., 2018; Brancato et al., 2020). The pharmaceutical companies require novel approach to face the lack of efficacy of the current models to assess the anti-cancer agents (Hickman et al., 2014; Lovitt et al., 2016). The present model aims to be a leap toward the adoption of 3D *in vitro* model as platform for drug testing in the preclinical studies. In this work, we propose a 3D-BCM (3D-breast cancer model) where breast cancer cells and mammary normal fibroblasts are seeded together on a tridimensional scaffold. Co-culturing different types of cells gives the opportunity to analyze the interaction between tumor and stroma counterpart. In this work, we exploited the potential of silk fibroin from mulberry silkworm as biomaterial to build a support for tumor cells growth. We have developed an off-the-shelf scaffold that maintains its features for long periods and the work has been focused to investigate how the thickness of the scaffolds effects the re-creation of tumor micro-niche and drug sensitivity (**Figure 8**). Natural silk protein fibroin is an interesting and versatile biomaterial. The process to obtain silk fibroin is straightforward and standardized, which makes this biomaterial quite appealing for biomedical applications (Kundu et al., 2014). Different matrices can be obtained in aqueous solution. Fibroin is used for different range of tissue engineering, regenerative medicine and stem cell research applications, due to its certain important features being protein biopolymer like robust mechanical properties, resilient, biodegradable, low immunogenic response and biocompatibility (Vepari and David Kaplan, 2007; Omenetto and Kaplan, 2010; Kundu et al., 2014; Benam et al., 2015; Rnjak-Kovacina et al., 2015; Pradhan et al., 2016; Yan et al., 2016; Holland et al., 2019). For the fabrication of different scaffolds silk fibroin can be used alone (Talukdar and Kundu, 2012) or in combination with collagen (Khoo et al., 2019), chitosan (She et al., 2008), gellan gum (Kundu et al., 2019) in order to fabricate scaffolds and recapitulate the tumor microenvironment. In addition, the natural source of fibroin is obtained from the mulberry silkworm cocoons (*Bombyx mori*), which are available abundantly and cost-effective in comparison to collagen or other exogenous extracellular matrices used to prepare scaffolds. Silk fibroin is widely used to fabricate *in vitro* different disease models (Kundu et al., 2013a, 2019; Sitarski et al., 2018) including breast cancer one (Wang et al., 2010; Talukdar and Kundu, 2012; Khoo et al., 2019). The tunings of the certain properties like mechanical and degradation are possible (Koh et al., 2015; Holland et al., 2019) as well as the regenerations of different types of tissues (Kundu et al., 2013b; Li et al., 2020). The porosity of the scaffold allows the cancer cell to grow as cluster in a three dimensional structure, resembling the tumor niche (Kundu et al., 2019). Ice-crystals act as porogen during the preparation of silk fibroin scaffolds. The large volume of solution takes more time to freeze, imparting a relatively large crystal size in thicker scaffolds (2 mm) compared to thinner one (1 mm). However, the pore-micro-architecture of both scaffolds is in well-agreement with the porous network of collagen-derived matrices, which is popularly used to investigate breast cancer cells invasion (Sapudom et al., 2015). The aforementioned study indicates least impact of pore sizes on morphology and behavior of breast cancer cells in 3D. Interconnectivity of sponges is linked with cellular distribution and is imparted by the interlocking phenomena of ice-crystals during freezing of silk fibroin solution. By adjusting the concentration of silk solution into designed biomaterials, the release of the drug can be manipulated (Seib et al., 2013). However, to our best of knowledge, this is the first report depicting the different release of drugs based on the thickness

of silk materials. The adsorption of doxorubicin is facilitated by the hydrophobic core of silk as indicated by the binding affinity, which in turn depends on crystallinity (Omenetto and Kaplan, 2010). Therefore, the higher the amount of β-sheet within the porous silk sponges, greater is the loading efficacy and slower is the release. This is observed in our present findings (**Figure 3A**). Silk fibroin being autofluorescent in nature also appear green in DOX free samples (Amirikia et al., 2018). The incorporation of DOX increase the noise, leading to blur fluorescent images. The systematic release of DOX from silk fibroin hydrogels is previously investigated (Seib et al., 2013). It has indicated the impact of weight percentage of silk on drug release. It suggests that 2 wt % of silk provide the highest cumulative release. Therefore, the choice of 2 wt % of SF sponge to model the drug screening platform in the present study is rational. DOX is considered as a model drug in the present study in order to interpret the diffusion of therapeutic molecules through the silk fibroin scaffold, which is further envisioned as low-cost drug screening platform. However, the cross-reactivity of the therapeutic molecules with silk fibroin is needed to be considered and should be investigated systematically for each case.

In this model, commercially available human breast cancer cells and mammary primary fibroblasts are seeded onto 1 or 2 mm silk fibroin scaffolds. In particular, the human mammary primary fibroblasts mimic the tumor stromal counterpart in the 3D-BCM. Two breast cancer cell lines types (luminal and basal phenotype) (Holliday and Speirs, 2011) are coupled with normal fibroblasts in order to recapitulate different subtype of breast cancer microenvironment. The proposed model is not the first in terms of co-culture of tumor and stromal cells (Wang et al., 2010; Hickman et al., 2014; Santo et al., 2016; Brancato et al., 2017a; Dondajewska et al., 2018). However, it shows that the heterotypic model is in the right roadmap toward the fabrication of a functional and efficient 3D tumor model. Other 3D tumor models based on solid porous scaffolds do not take into account of the stromal component (Talukdar and Kundu, 2012; Kundu et al., 2013a; Brancato et al., 2017b). Recently, myofibroblasts or cancer activated fibroblasts (CAF) are considered important player in triggering tumoral progression (Beacham and Cukierman, 2005; Cirri and Chiarugi, 2012; Lovitt et al., 2016; Alguacil-Núñez et al., 2018). Fibroblasts have dual role in tissues. In normal condition, fibroblasts protect the tissues from the cancer cells invasion and proliferation (Werb and Lu, 2016). In stress condition caused by wound or during tumorigenesis, the paracrine loop between cancer cells and fibroblasts triggers the stromal cells transformation, activating the fibroblasts. This phenomenon is known as stromagenesis and runs in parallel with the tumor progression (Castelló-Cros and Cukierman, 2009; Lu et al., 2012; Werb and Lu, 2016). The 3D-BCM proposed in this work is able to capture the evolution of the tumor microenvironment from the initial step where the cancer cells modify the tumor surrounding. Further investigations should assess if the tumor microenvironment transformation is due to the direct contact of the cells or mediated by soluble factors. Our results in terms of cell proliferation in the scaffold are aligned with other previous results where the cells in the scaffolds are metabolically active during the period of 14 days chosen for the model (Brancato et al., 2017a). It is also noteworthy to highlight that the cells in homotypic models are less proliferative when compared to the heterotypic conditions. This shows an interaction among the cell type in the promotion of cell viability and proliferation. Breast cancer cells in the 3D scaffold show a rounded shape, and fibroblast are less elongated than the usual morphology they exhibit in 2D culture. This is highlighted by the SEM and fluorescence images. Histological staining shows that cancer cells copycat the acinar spheroid-like structure. This morphological profile has already recapitulated in previous works (Wang et al., 2010; Talukdar and Kundu, 2012; Wang and Kaplan, 2012; Kundu et al., 2013a). The spheroid architecture is the most resembling tumor spatial organization *in vivo*. ECM secreted by CAF has also a peculiar profile characterized by the over-expression of MMP's, Col I, and fibronectin among the others. Those genes are hallmark for fibrotic phenotype in solid cancers (Bornstein and Sage, 2002; Wong and Rustgi, 2013). Our results state the overexpression of tumor microenvironment markers when the fibroblasts are co-cultured with cancer cells. The up-regulation of MMPs is extremely important features to recapitulate as they play a relevant role in the remodeling of tumor microenvironment. Moreover, our model showed that cancer cells could stimulate the production of collagen by fibroblasts. The CAFs are also investigated as target for anti-cancer agents due to their sophisticated crosstalk between cancer cells and stroma (Zhuo et al., 2009; Conklin and Keely, 2012; Quail and Joyce, 2013). It has also been demonstrated that 3D *in vitro* tumor platform recapitulate better the drug-response. This has been shown when stroma or tumor microenvironment is included in the models (Ridky et al., 2010; Peck and Wang, 2013; Lovitt et al., 2016; Brancato et al., 2017c, 2018). In this work, the use of two different thicknesses to fabricate 3D-BCM also affects the drug response. Based on previous studies (Brancato et al., 2018; Dondajewska et al., 2018) and considering the morphology and thickness of the scaffolds, we selected two different DOX concentrations to carry out our drug-response tests. We have found that 2 mm SF scaffold has retained DOX for a longer time and the release has been slower as compared to the 1 mm SF scaffold. The 2 mm scaffold's behavior has affected the inhibition of proliferation and metabolic activity after DOX treatment. It may be postulated that DOX is entrapped in the scaffold for a longer period, which might have been available for the cells during the 72 h of treatment. The differences in DOX release may be referred to the size of scaffold and the capability to embed more liquid solution. In our opinion, the scaffold thickness is relevant to recapitulate the tumor microenvironment and to make the drug-screening tool more reliable. In this work, the 2 mm scaffold can be considered the best choice for further investigation because allows a slower DOX release and it is able to reduce the cellular metabolic activity and proliferation, better than the 1 mm SF scaffold. 3D-BCM proposed in this work is suitable for drug screening. This model may also support the possibility to perform proliferation assays as well as an easy histological sample preparation along with the gene expression analysis. These are strong advantages of this model toward further characterization for the use as testing platform for anti-cancer drug screening. Bioengineered

cancer models are a valid support to preclinical studies. In this work, we demonstrate that heterotypic 3D *in vitro* cancer model may unravel the crosstalk between cancer cells and tumor microenvironment. We consider that the sample size of the experimental set-up is less, however, previous works demonstrate the reproducibility of the results when SF freeze-dried matrices are used (Talukdar and Kundu, 2012; Kundu et al., 2013a). In future, other cancer types characterized by a fibrotic stroma can be recapitulated using SF scaffolds as lung, colon or pancreatic cancer. The system can be improved by adding endothelial or immune cells in order to investigate the complexity of the tumor microenvironment. In the near future, patient-derived cancer and stromal cells can be seeded onto silk fibroin scaffold to fabricate a 3D-BCM for personalized drug testing. In conclusion, the developed 3D breast cancer model makes closer for the complete understanding of the mechanisms underpinning breast cancer progression.

CONCLUSION

The proposed *in vitro* breast cancer model aims to be used as a tool for drug screening or for investigating tumor microenvironment. Silk protein fibroin scaffold allows us to grow both fibroblasts and cancer cells, which can facilitate the investigation of the tumor-stroma crosstalk as well as cell-extracellular matrix interactions. These interactions are necessary for tumor growth and invasion. This model enlightens the mechanism of tumor migration, cancer associated fibroblast transformation and extracellular matrix remodeling. The model is also a straightforward 3D platform for drug testing due to its easy-to-use and cost-effective features. The interconnectivity and stability of the platform is envisioned to study the invasion of cancer cells over prolong time. The 3D breast cancer model proposed may also be useful for better understanding of the mechanisms behind chemoresistance and metastatic spread.

DATA AVAILABILITY STATEMENT

The datasets generated for this study are available on request to the corresponding author.

AUTHOR CONTRIBUTIONS

VB and SK designed and coordinated the study. VB performed the experiments, analysis of data, and wrote the manuscript. BK performed silk fibroin extraction, scaffold preparation, analyses, and participated in writing the manuscript. All authors read, revised, and approved the final manuscript.

FUNDING

This work was supported by EU-Horizon 2020 grant FoReCaST—Forefront Research in 3D Disease Cancer Models as *in vitro* Screening Technologies (H2020-WIDESPREAD-2014-668983). The authors also acknowledge the FRONTHERA project (Frontiers of technology for theranostics of cancer, metabolic and neurodegenerative diseases) (NORTE-01-0145-FEDER-0000232) and Fundaçao ciencia e tecnologia (FCT grant agreement: PTDC/BTM-ORG/28168/2017 to VB and SK).

ACKNOWLEDGMENTS

We acknowledge the excellent technical assistance provided by Ms. Teresa Oliveira for sectioning and staining of the silk fibroin scaffold for this work. We also thank Dr. Elsa Ribeiro and Dr. Isabel Leonor for the precious support for the SEM microscopy.

SUPPLEMENTARY MATERIAL

The Supplementary Material for this article can be found online at: https://www.frontiersin.org/articles/10.3389/fmats.2020.00116/full#supplementary-material

REFERENCES

Alguacil-Núñez, C., Ferrer-Ortiz, I., García-Verd,ú, E., López-Pirez, P., Llorente-Cortijo, I. M., and Sainz, B. (2018). Current perspectives on the crosstalk between lung cancer stem cells and cancer-associated fibroblasts. *Crit. Rev. Oncol. Hematol.* 125, 102–110. doi: 10.1016/j.critrevonc.2018.02.015

Altrock, P. M., Yoon, N., Bull, J. A., Wu, H., Ruiz-Ramírez, J., Miroshnychenko, D., et al. (2018). The impact of tumor stromal architecture on therapy response and clinical progression. *BioRxiv*. 451047. doi: 10.1101/451047

Amirikia, M. S.,Shariatzadeh, M. A. S., Jorsaraei, G. A., and Mehranjani, M. S. (2018). Auto-fluorescence of a silk fibroin-based scaffold and its interference with fluorophores in labeled cells. *Eur. Biophys. J.* 47, 573–581. doi: 10.1007/s00249-018-1279-1

Arya, N., Sardana, V., Saxena, M., Rangarajan, A., and Katti, D. S. (2012). Recapitulating tumour microenvironment in chitosan – gelatin three-dimensional scaffolds: an improved in vitro tumour model. 9, 3288–3302. doi: 10.1098/rsif.2012.0564

Beacham, D. A., and Cukierman, E. (2005). Stromagenesis: The changing face of fibroblastic microenvironments during tumor progression. *Semin. Cancer Biol.* 15, 329–341. doi: 10.1016/j.semcancer.2005.05.003

Benam, K. H., Dauth, S., Hassell, B., Herland, A., Jain, A., Jang, K.-J., (2015). Engineered in vitro disease models. *Annu. Rev. Pathol. Mech. Dis.* 10, 195–262. doi: 10.1146/annurev-pathol-012414-040418

Bornstein, P., and Sage, H. (2002). Matricellular proteins : extracellular modulators of cell function, Curr. *Opin. Cell Biol.* 14, 608–616. doi: 10.1016/S0955-0674(02)00361-7

Brancato, V., Comunanza, V., Imparato, G., Cor,à, D., Urciuolo, F., Noghero, A., et al. (2017a). Bioengineered tumoral microtissues recapitulate desmoplastic reaction of pancreatic cancer. *Acta Biomater.* 49, 152–166. doi: 10.1016/j.actbio.2016.11.072

Brancato, V., Gioiella, F., Imparato, G., Guarnieri, D., Urciuolo, F., and Netti, P. A. (2018). 3D Breast Cancer Microtissue reveals the role of tumor microenvironment on the transport and efficacy of free-Doxorubicin in vitro. *Acta Biomater.* 75, 200–212. doi: 10.1016/j.actbio.2018.05.055

Brancato, V., Gioiella, F., Profeta, M., Imparato, G., Guarnieri, D., Urciuolo, F., et al. (2017c). 3D tumor microtissues as an in vitro testing platform for microenvironmentally-triggered drug delivery systems. *Acta Biomater.* 57, 47–58. doi: 10.1016/j.actbio.2017.05.004

Brancato, V., Oliveira, J. M., Correlo, V. M., Reis, R. L., and Kundu, S. C. (2020). Could 3D models of cancer enhance drug screening? *Biomaterials* 232:119744. doi: 10.1016/j.biomaterials.2019.119744

Brancato, V., Ventre, M., Imparato, G., Urciuolo, F., Meo, C., and Netti, P. A. (2017b). A straightforward method to produce decellularized dermis-based matrices for tumour cell cultures. *J. Tissue Eng. Regen. Med*. 12, e71–e81. doi: 10.1002/term.2350

Caballero, D., Kaushik, S., Correlo, V. M., Oliveira, J. M., Reis, R. L., and Kundu, S. C. (2017). Organ-on-chip models of cancer metastasis for future personalized medicine: From chip to the patient. *Biomaterials*. 149, 98–115. doi: 10.1016/j.biomaterials.2017.10.005

Cacicedo, M., León, I. E., Gonzalez, J. S., Porto, L., et al. (2016). Modified bacterial cellulose scaffolds for localized doxorubicin release in human colorectal HT-29 cells. *Colloids Surfaces B Biointerfaces*. 140, 421–429. doi: 10.1016/j.colsurfb.2016.01.007

Castelló-Cros, R., and Cukierman, E. (2009). Stromagenesis during tumorigenesis: characterization of tumor- associated fibroblasts and stroma-derived 3D matrices. *Methods Mol Biol.* 522, 275–305. doi: 10.1007/978-1-59745-413-1_19

Cirri, P., and Chiarugi, P. (2012). Cancer-associated-fibroblasts and tumour cells: a diabolic liaison driving cancer progression. *Cancer Metastasis Rev*. 31, 195–208. doi: 10.1007/s10555-011-9340-x

Conklin, M. W., and Keely, P. J. (2012). Why the stroma matters in breast cancer. *Cell Adhes. Migr*. 6286, 249–260. doi: 10.4161/cam.20567

Dondajewska, E., Juzwa, W., Mackiewicz, A., and Dams-Kozlowska, H. (2018). Heterotypic breast cancer model based on a silk fibroin scaffold to study the tumor microenvironment. *Oncotarget* 9, 4935–4950. doi: 10.18632/oncotarget.23574

European Commission (2016). *Cancer Statistics - Specific Cancers*. Brussels: European Commission, 1–16.

Ferreira, L. P., Gaspar, V. M., and Mano, J. F. (2018). Design of spherically structured 3D in vitro tumor models -Advances and prospects. *Acta Biomater*. 75, 11–34. doi: 10.1016/j.actbio.2018.05.034

Fiori, M. E., Di Franco, S., Villanova, L., Bianca, P., Stassi, G., and De Maria, R. (2019). Cancer-associated fibroblasts as abettors of tumor progression at the crossroads of EMT and therapy resistance. *Mol. Cancer*. 18, 1–16. doi: 10.1186/s12943-019-0994-2

Hickman, J. A., Graeser, R., de Hoogt, R., Vidic, S., Brito, C., Gutekunst, M., et al. (2014). Imi Predect consortium, Three-dimensional models of cancer for pharmacology and cancer cell biology: Capturing tumor complexity in vitro/ex vivo. *Biotechnol. J*. 9, 1115–1128. doi: 10.1002/biot.201300492

Holland, C., Numata, K., Rnjak-Kovacina, J., and Seib, F. P. (2019). The biomedical use of silk: past, present. *Future, Adv. Healthc. Mater*. 8:e1800465. doi: 10.1002/adhm.201800465

Holliday, D. L., and Speirs, V. (2011). Choosing the right cell line for breast cancer research. *Breast Cancer Res*. 13:215. doi: 10.1186/bcr2889

Khoo, A. S., Valentin, T. M., Leggett, S. E., Bhaskar, D., Bye, E. M., Benmelech, S., et al. (2019). Breast cancer cells transition from mesenchymal to amoeboid migration in tunable three-dimensional silk-collagen hydrogels. *ACS Biomater. Sci. Eng*. 5, 4341–4354. doi: 10.1021/acsbiomaterials.9b00519

Klein-Goldberg, A., Maman, S., and Witz, I. P. (2014). The role played by the microenvironment in site-specific metastasis. *Cancer Lett*. 352, 54–58. doi: 10.1016/j.canlet.2013.08.029

Koh, L. D., Cheng, Y., Teng, C. P., Khin, Y. W., Loh, X. J., Tee, S. Y., et al. (2015). Structures, mechanical properties and applications of silk fibroin materials. *Prog. Polym. Sci*. 46, 86–110. doi: 10.1016/j.progpolymsci.2015.02.001

Kundu, B., Kurland, N. E., Bano, S., Patra, C., Engel, F. B., Yadavalli, V. K., et al. (2014). Silk proteins for biomedical applications: Bioengineering perspectives. *Prog. Polym. Sci*. 39, 251–267. doi: 10.1016/j.progpolymsci.2013.09.002

Kundu, B., Rajkhowa, R., Kundu, S. C., and Wang, X. (2013b). Silk fibroin biomaterials for tissue regenerations. *Adv. Drug Deliv. Rev*. 65, 457–470. doi: 10.1016/j.addr.2012.09.043

Kundu, B., Saha, P., Datta, K., and Kundu, S. C. (2013a). A silk fibroin based hepatocarcinoma model and the assessment of the drug response in hyaluronan-binding protein 1 overexpressed HepG2 cells. *Biomaterials*. 34, 9462–9474. doi: 10.1016/j.biomaterials.2013.08.047

Kundu, B. A., Bastos, R. F., Brancato, V., Cerqueira, M. T., Oliveira, J. M., Correlo R. L., et al. (2019). Mechanical property of hydrogels and the presence of adipose stem cells in tumor stroma affect spheroid formation in the 3D osteosarcoma model. *ACS Appl. Mater. Interfaces*. 11, 14548–14559. doi: 10.1021/acsami.8b22724

Li, C., Guo, C., Fitzpatrick, V., Ibrahim, A., Zwierstra, M. J., Hanna, P., et al. (2020). Design of biodegradable, implantable devices towards clinical translation. *Nat. Rev. Mater*. 5, 61–81. doi: 10.1038/s41578-019-0150-z

Li, J., Zhou, Y., Chen, W., Yuan, Z., You, B., Liu, Y., et al. (2018). A novel 3D in vitro tumor model based on silk fibroin/chitosan scaffolds to mimic the tumor microenvironment. *ACS Appl. Mater. Interfaces.* 10, 36641–36651. doi: 10.1021/acsami.8b10679

Livak, K. J., and Schmittgen, T. D. (2001). Analysis of relative gene expression data using real-time quantitative PCR and the 2-ΔΔCT method. *Methods* 25, 402–408. doi: 10.1006/meth.2001.1262

Lovitt, C. J., Shelper, T. B., and Avery, V. M. (2016). Cancer drug discovery: recent innovative approaches to tumor modeling. *Expert Opin. Drug Discov*. 11, 885–894. doi: 10.1080/17460441.2016.1214562

Lu, P., Weaver, V. M., and Werb, Z. (2012). The extracellular matrix: a dynamic niche in cancer progression. *J. Cell Biol*. 196, 395–406. doi: 10.1083/jcb.201102147

Madar, S., Goldstein, I., and Rotter, V. (2013). "Cancer associated fibroblasts" - more than meets the eye. *Trends Mol. Med*. 19, 447–453. doi: 10.1016/j.molmed.2013.05.004

Miles, F. L., and Sikes, R. A. (2014). Insidious changes in stromal matrix fuel cancer progression. *Mol. Cancer Res*. 12, 297–312. doi: 10.1158/1541-7786.MCR-13-0535

Omenetto, F. G., and Kaplan, D. L. (2010). New opportunities for an ancient material. *Science* 329, 528–531. doi: 10.1126/science.1188936

Östman, A. (2012). The tumor microenvironment controls drug sensitivity. *Nat. Med*. 18, 1332–1334. doi: 10.1038/nm.2938

Peck, Y., and Wang, A.-D. (2013). Three-dimensionally engineered biomimetic tissue models for *in vitro* drug evaluation: delivery, efficacy and toxicity. *Expert Opin. Drug Deliv*. 10, 369–383. doi: 10.1517/17425247.2013.751096

Pradhan, S., Hassani, I., Clary, J. M., and Lipke, E. A. (2016). Polymeric biomaterials for in vitro cancer tissue engineering and drug testing applications. *Tissue Eng. Part B Rev*. 22, 470–484. doi: 10.1089/ten.teb.2015.0567

Qu, Y., Dou, B., Tan, H., Feng, Y., Wang, N., and Wang, D. (2019). Tumor microenvironment-driven non-cell-autonomous resistance to antineoplastic treatment. *Mol. Cancer*. 18, 1–16. doi: 10.1186/s12943-019-0992-4

Quail, D. F., and Joyce, J. A. (2013). Microenvironmental regulation of tumor progression and metastasis. *Nat. Med*. 19, 1423–1437. doi: 10.1038/nm.3394

Ridky, T. W., Chow, J. M., Wong, D. J., and Khavari, P. A. (2010). Invasive three-dimensional organotypic neoplasia from multiple normal human epithelia. *Nat. Med*. 16, 1450–1456. doi: 10.1038/nm.2265

Rnjak-Kovacina, J., Wray, L. S., Burke, K. A., Torregrosa, T., Golinski, J. M., Huang, W., et al. (2015). Lyophilized silk sponges: a versatile biomaterial platform for soft tissue engineering. *ACS Biomater. Sci. Eng*. 1, 260–270. doi: 10.1021/ab500149p

Rodrigues, T., Kundu, B., Silva-Correia, J., Kundu, S. C., Oliveira, J. M., Reis, R. L., et al. (2018). Emerging tumor spheroids technologies for 3D in vitro cancer modeling. *Pharmacol. Ther*. 184, 201–211. doi: 10.1016/j.pharmthera.2017.10.018

Santo, V. E., Estrada, M. F., Rebelo, S. P., Abreu, S., Silva, I., Pinto, C., et al. (2016). Adaptable stirred-tank culture strategies for large scale production of multicellular spheroid-based tumor cell models. *J. Biotechnol*. 221, 118–129. doi: 10.1016/j.jbiotec.2016.01.031

Sapudom, J., Rubner, S., Martin, S., Kurth, T., Riedel, S., Mierke, C. T., et al. (2015). The phenotype of cancer cell invasion controlled by fibril diameter and pore size of 3D collagen networks. *Biomaterials* 52, 367–375. doi: 10.1016/j.biomaterials.2015.02.022

Seib, P., Pritchard, E. M., and Kaplan, D. L. (2013). Self-assembling doxorubicin silk hydrogels for the focal treatment of primary breast cancer. *Adv. Funct. Mater*. 23, 56–58. doi: 10.1002/adfm.201201238

Senkus, E., Kyriakides, S., Ohno, S., Penault-Llorca, F., Poortmans, P., Rutgers, E., et al. (2015). Primary breast cancer: ESMO Clinical Practice Guidelines for diagnosis, treatment and follow-up. *Ann. Oncol*. 26, v8–v30. doi: 10.1093/annonc/mdv298

She, Z., Jin, C., Huang, Z., Zhang, B., Feng, Q., and Xu, Y. (2008). Silk fibroin/chitosan scaffold: Preparation, characterization, and culture with HepG2 cell. *J. Mater. Sci. Mater. Med*. 19, 3545–3553. doi: 10.1007/s10856-008-3526-y

Sitarski, A. M., Fairfield, H., Falank, C., and Reagan, M. R. (2018). 3D tissue engineered in vitro models of cancer in bone. *ACS Biomater. Sci. Eng*. 4, 324–336. doi: 10.1021/acsbiomaterials.7b00097

Soysal, S. D., Tzankov, A., and Muenst, S. E. (2015). Role of the tumor microenvironment in breast cancer. *Pathobiology* 82, 142–152. doi: 10.1159/000430499

Spill, F., Reynolds, D. S., Kamm, R. D., and Zaman, M. H. (2016). Impact of the physical microenvironment on tumor progression and metastasis. *Curr. Opin. Biotechnol*. 40, 41–48. doi: 10.1016/j.copbio.2016.02.007

Stadler, M., Walter, S., Walzl, A., Kramer, N., Unger, C., Scherzer, M., et al. (2015). Increased complexity in carcinomas: Analyzing and modeling the interaction of human cancer cells with their microenvironment. *Semin. Cancer Biol*. 35, 107–124. doi: 10.1016/j.semcancer.2015.08.007

Talukdar, S., and Kundu, S. C. (2012). A non-mulberry silk fibroin protein based 3D in vitro tumor model for evaluation of anticancer drug activity. *Adv. Funct. Mater*. 22, 4778–4788. doi: 10.1002/adfm.201200375

Tao, Z. Q., Shi, A., Lu, C., Song, T., Zhang, Z., and Zhao, J. (2015). Breast cancer: epidemiology and etiology. *Cell Biochem. Biophys*. 72, 333–338. doi: 10.1007/s12013-014-0459-6

Vepari, C., and David Kaplan, L. (2007). Silk as biomaterial. *Prog. Polym. Sci*. 100, 130–134. doi: 10.1016/j.progpolymsci.2007.05.013

Wang, X., and Kaplan, D. L. (2012). Hormone-responsive 3D multicellular culture model of human breast tissue. *Biomaterials* 33, 3411–3420. doi: 10.1016/j.biomaterials.2012.01.011

Wang, X., Sun, L., Maffini, M., and V., Soto, A. (2010). Sonnenschein, C., Kaplan, D. L., A complex 3D human tissue culture system based on mammary stromal cells and silk scaffolds for modeling breast morphogenesis and function. *Biomaterials* 31, 3920–3929. doi: 10.1016/j.biomaterials.2010.01.118

Werb, Z., and Lu, P. (2016). The role of stroma in tumor development. *Cancer J*. 21, 250–253. doi: 10.1097/PPO.0000000000000127

Wong, G. S., and Rustgi, A. K. (2013). Matricellular proteins: Priming the tumour microenvironment for cancer development and metastasis. *Br. J. Cancer*. 108, 755–761. doi: 10.1038/bjc.2012.592

Yan, P.-L., Silva-Correia, J., Ribeiro, V. P., Miranda-Gonçalves, V., Correia, C., da Silva Morais, A., et al. (2016). Tumor growth suppression induced by biomimetic silk fibroin hydrogels. *Sci. Rep*. 6:31037. doi: 10.1038/srep31037

Yuan, Y., Jiang, Y. C., Sun, C. K., and Chen, Q. M. (2016). Role of the tumor microenvironment in tumor progression and the clinical applications (Review). *Oncol. Rep*. 35, 2499–2515. doi: 10.3892/or.2016.4660

Zhuo, S., Chen, J., Xie, S., Hong, Z., and Jiang, X. (2009). Extracting diagnostic stromal organization features based on intrinsic two-photon excited fluorescence and second-harmonic generation signals. *J. Biomed. Opt*. 14, 020503. doi: 10.1117/1.3088029

Conflict of Interest: The authors declare that the research was conducted in the absence of any commercial or financial relationships that could be construed as a potential conflict of interest.